World Journal of Advanced Research and Reviews
eISSN: 2581-9615 CODEN (USA): WJARAI
Cross Ref DOI: 10.30574/wjarr
Journal homepage: https://wjarr.com/

(RESEARCH ARTICLE)

Check for updates

Ecological production of silver nanoparticles using extract from *Chrozophora plicata* leaves for improved anticorrosion and antibacterial use

Madhanraj Lakshmanan [1,*], Kasthuri Periyaiya Kannaiah [2] and Jaya Pradeep Gunasekaran [2]

[1] *Department of Chemistry, LRG College of Arts and Science for Women, Tirupur, Tamilnadu, India.*
[2] *Department of Chemistry, Government Arts College (Autonomous), (Affiliated to Bharathiar University), Coimbatore-641018, India.*

World Journal of Advanced Research and Reviews, 2025, 28(01), 2069-2085

Publication history: Received on 18 September 2025; revised on 24 October 2025; accepted on 28 October 2025

Article DOI: https://doi.org/10.30574/wjarr.2025.28.1.3645

Abstract

The current work generated silver nanoparticles by green synthesis from the extract of Chrozophora Plicata (CP) leaves extracted at room temperature with a pH range between 10 and 12, after years of continuous work in the bottom-up technique and biological Ag nanoparticle manufacturing. Using a range of characterisation techniques, the generated Ag Nps form and phase purity were carefully investigated. According to the phyto chemical activities of Chrozophora Plicata (CP) leaf extract, quercetin, one of the primary flavonoid components, increases the conversion of Ag+ to Ag0. Ag Nps' antibacterial efficacy against S. aureus and E. coli was also assessed. The outcomes show that Ag Nps have strong antibacterial qualities against the E. coli bacteria.

Keywords: Anticorrosion; Silver nanoparticle; Antibacterial; SEM

1. Introduction

Because of its unique advancements, nanotechnology has a wide range of exciting applications and can readily integrate with other technologies with a few tweaks. Numerous industries, including the environment, medicine, textiles, biotechnology, agriculture, food, energy, and medication delivery, have benefited from the increased surface area and faster reaction rate that nanostructured materials have made possible [1]. These materials have a high grain boundary volume percentage and are fine-grained [2]. Numerous materials and methods have been used to create a variety of nanoparticles [3–5]. The intended end usage determines the synthesis material. Because plant-mediated materials are cheap and non-toxic, researchers have recently created nanoparticles from plant biomasses [6]. Nanoparticles derived from plants have been used in several fields, most recently as chemicals in oilfields [7–11]. The industry uses oilfield chemicals for hydrocarbon production, completions, and drilling. In order to eliminate harmful gasses and regulate fluid loss and wellbore stability, nanoparticulates have been added to drilling mud [12,13]. Cement spacers and cement properties enhancers have been designed at the nanoscale [14,15]. Other oilfield chemicals for production and enhanced recovery have been designed in the nanoscale, including corrosion inhibitors and surfactants [16].

Green nano synthesis is valuable due to the rate of mutation, antibiotic resistance, and the efficacy of microbial infections. Proteins, amino acids, alkaloids, and other natural metabolites are examples of plant biomolecules that are crucial for comprehending the synthesis and structural alterations of Ag Nps. Various silver nanoparticles, such as silver, gold, zinc, and others, are made from extracts of plant parts [17]. Due to their high toxicity, physical and chemical methods of producing nanoparticles [18] have limited advantages. Due to the down streaming process, the method is costly and necessitates a large energy input [19]. Green chemistry is a safe and economical approach, as the earlier articles have stated. A precursor to the synthesis of Ag Nps and secondary metabolites is silver nitrate and

* Corresponding author: Madhanraj Lakshmanan

phytocompounds necessary for reducing Ag+ to Ag^0. However, there are no reports of the biosynthesis of the same silver nanoparticles with distinct biological and electrochemical uses. Nonetheless, reports of the biosynthesis of silver nanoparticles for various uses in the realm of anticorrosion activities have been made [20]. Ag nanoparticles are reduced by using cow urine. Ag nanoparticles that have been biosynthesized are powerful catalysts for organic transformation processes. They have been effectively employed as a photocatalyst to break down dangerous organic dyes including crystal violet and methylene blue [63]. The E. coli bacteria is an invasive aquatic plant species that negatively impacts human health and the environment [21–24]. This is regarded as biomass for the production of biopesticides, fertilizers, animal feed, energy sources, and water treatment. This is considered as biomass for generating energy sources, fertilizers, animal feeds, water treatment, and biopesticide [25] Belonging to the family Pontendericeae, its plant taxonomy shows that, walls of these cells are composed of ferulic acid.

Many studies have shown that silver nanoparticles have antibacterial properties, which motivated us to determine this property of Ag NPs. The results of a study that used S. aureus and E. coli bacteria to investigate the bacterial activity of Ag NPs are presented in this article. Furthermore, in the hydrochloric acid system, an electrochemical reaction takes place in the steel's active regions when it is exposed to corrosive substances [33]. Iron metal is necessary for nuclear power, pipeline construction, transportation, and chemical processing. A variety of methods, including coatings, paints, cathodic and anodic protection, and corrosion inhibitors, were employed to stop the steel corrosion process. Because of their ease of installation and high effectiveness in preventing metal corrosion, corrosion inhibitors are recommended [21, 34–37]. In industrial, hydrochloric acid solution is frequently used to clean metal surfaces of contaminants. The high use of hydrochloric acid solution over time leads to the breakdown of the iron surface. Because of their high adsorption rate, inhibitors are becoming more and more popular in both the academic and industrial sectors. The main factors influencing the adsorption process are the corrosive solution, temperature, and electrochemical potential in the Fe-HCl solution-metal line edge, as well as the physical, chemical, and active properties of the inhibitor species. Environmental laws and rules limit the use of synthetic corrosion inhibitors due to their negative environmental effects, which drives up the cost of various industrial units. This promotes the creation of effective and non-toxic corrosion-inhibiting species [13,22,38–42]. Information on corrosion control techniques is given in Table 1. Understanding the structure of customized nanoparticles and preserving the precursor and reaction conditions help determine their efficacy.

Table 1 Methods of corrosion control

Control method	Description
Corrosion inhibitors	Concentrations to a corrosive system to reduce electrochemical process.
Electrical protection	The metal corrosion can be prevented by small potential differences between anode and cathode.
Excellent equipment Design (EED)	EED prevents the corrosion of the metals by avoiding galvanic corrosion (the two dissimilar metals connection in the corrosive)
Surface coating	It involves use of protective coatings to generate the physical barrier between metal and corrosive system
Material selection	The metal having high mechanical strength should be selected

It is anticipated that the green nanoparticles derived from the plant species will exhibit good corrosion protection properties for a variety of metals in a range of corrosive conditions, whether they are basic or acidic, and at varying concentrations. There is, however, no particular report on the use of iron as an anti-corrosion agent for iron metal in a 1M HCl solution. In light of this, the CP plant's leaves were extracted in order to create silver nanoparticles for this investigation. FT-IR, PXRD, HRTEM, and UV/visible tests verified the production of silver nanoparticles from CP extract. Alternating current impedance spectroscopy was used to assess CP's corrosion inhibition effectiveness. Atomic Absorption Spectroscopy (AAS) and electrochemical methods were used to investigate the effectiveness of silver nanoparticles in preventing corrosion.

2. Materials and methods

Chrozophora Plicata is a native plant usually occurs in non-wetlands, but occasionally in wetlands (Fig. 1). Within 15 to 20 days, it spreads quickly and covers the surface of water bodies in a thick, floating mat. We collected fresh *Chrozophora Plicata* leaves from the Kanuvai (Coimbatore) in Tamilnadu. After convincingly washing the plant leaves with deionized

water to get rid of any debris that would contaminate the extract, they were ultimately allowed to dry in the sun. Agate mortar and pestle were used to grind the dried leaves. Using 50 g of powdered plant material (dry leaves) in 300 ml of acetone, the Soxhlet extraction was carried out for almost seven hours. The green chemical that was isolated was then filtered and kept in the refrigerator to avoid side reactions and contamination-free.

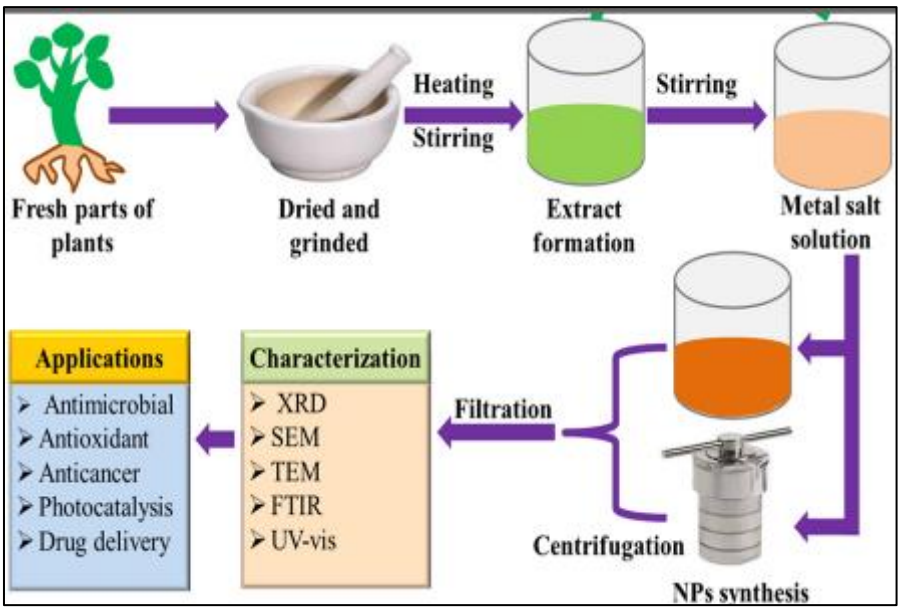

Figure 1 Chrozophora Plicata -plant extract figure

2.1. Phytochemical analysis

Reducing and stabilizing substances participate in the bottom-up process used in biological synthesis of nanoparticles. Phytochemical research reveals a variety of Phyto-moieties found in CP leaf extracts. The findings of the screening tests for qualitative analysis that were carried out at their lab for this purpose are listed in Table 2. These phytomedicines have a stimulating effect and function as a mild reducing agent when silver nitrate (Ag+) is reduced to silver (Ag^0) at the nanoscale. Additionally, it presents itself as a capping and stabilizing agent. The phytochemical analysis of *Chrozophora Plicata* leaves also revealed the presence of alkaloids, terpenoids, phenolics, flavonoids, and tannins. The highest concentration of flavonoids and a good proportion of 1H-Pyrazole-3-amine are found in water hyacinth, as was previously mentioned [43]. Chemical substances known as antioxidants protect cells from dangerous free radicals. The flavonoid concentration reduces the risk of cardiovascular diseases and a number of cancers.

One plant pigment that is particularly strong as an antioxidant flavonoid is quercetin. It is a beneficial antioxidant that can guard against a number of medication toxicities [44]. Flavonoids, such as 1H-Pyrazole-3-amine, were discovered to make up the majority of the phytochemicals. Silver ions are reduced to silver nanoparticles by the amine ($-NH_2$) groups of flavonoids, such as 1H-Pyrazole-3-amine. By moving protons from one location in the molecule to another, structural isomers known as tautomers are created. The hydrogen atom that is liberated during this enol to keto conversion process in 1H-Pyrazole-3-amine aids in the transformation of the ion into metallic silver nanoparticles and stabilizes the Ag Nps.

Table 2 Qualitative analysis of Phytochemical results shown by CP leaf extract

S.No	Metabolite	Test performed	Observation	Inference
1	Alkaloids	CP-extract with Mayer's reagent	Presence of White creamy precipitate	Presence of Alkaloids
		CP-extract with Dragendorff's reagent	Presence of reddish-brown precipitate	Presence of Alkaloids
2	Carbohydrates	CP-extract with α- naphthol in alcohol, two drops of þ concentrated sulphuric acid.	No violet ring	Absence of carbohydrates.

3	Flavonoids	Alkaline reagent test CP - leaf extract 10% ammonium hydroxide solution	Yellow fluorescence	flavonoids may be present
4	Sterols	CP-extract with CHCl3 + Acetic anhydride + Con.H2SO4	Absence of reddish-brown precipitate	Absence of sterols
5	Saponins	CP-extract shaken with water	Presence of foam	Presence of saponins
6	Cardiac glycosides	CP-extract with Baljet reagent	Presence of foam	Presence of Cardiac glycosides
7	Lignin	CP-extract with Aq.NaOH	Absence of yellow colour	Absence of Lignin
8	Coumarins	CP-extract with 10% NaOH and CHCl3	Presence of yellow colour	Presence of Coumarins

2.2. Synthesis of Ag Nps

The solution for the AR grade silver nitrate, which was acquired from SDFCL, a company based in Mumbai, was made with double-distilled water. 50 milliliters of CP extract and 200 milliliters of AgNO3 (0.01 N) were mixed in a 1:4 precursor to plant extract ratio. The production of nanoparticles is significantly influenced by pH. The alkaline pH of 9–11, which is suitable for the synthesis, also affected the color intensity of the aqueous solution. A lower concentration of silver nitrate is produced in this solution, whose pH was determined by CP extract to be 11, in order to investigate its hidden properties.

Following agitation and mixing, the reaction mixture was exposed to sunlight for approximately fifteen minutes. A distinct indication of the development of green silver nanoparticles or *Chrozophora Plicata* (CP) extract silver nanoparticles is provided by the colour shift from green to light brown to dark brown (Fig. 2).

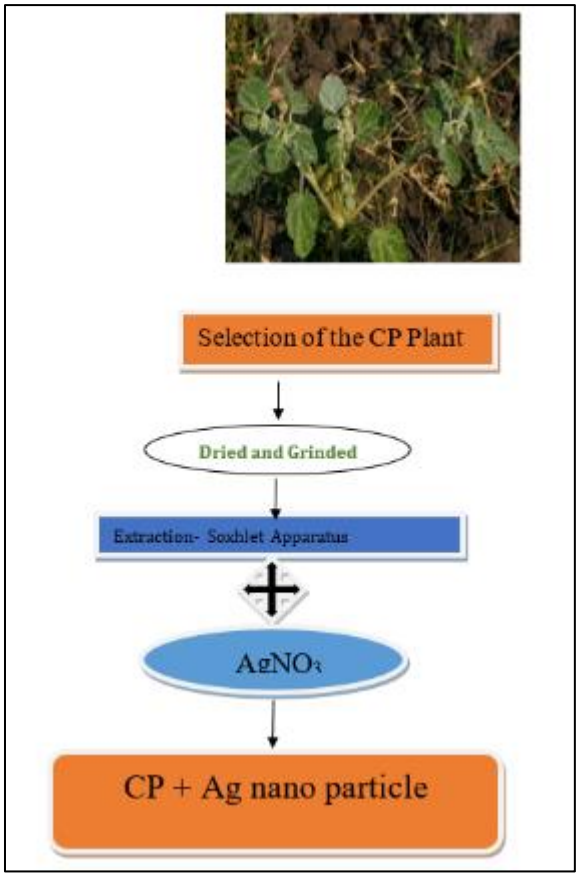

Figure 2 Schematic flow of green synthesis of Ag NPs by CP leaf extract -Soxhlet apparatus

Centrifugation was carried out for roughly 20 minutes at 1000 rpm while these green nanoparticles were contained in the centrifuge tubes. The brown residue that remains is then put into a clean China dish, and the colourless centrifuge is thrown away. To prevent the residue from charring, it is carefully dried over the hot plate at a reduced temperature (Fig.3).

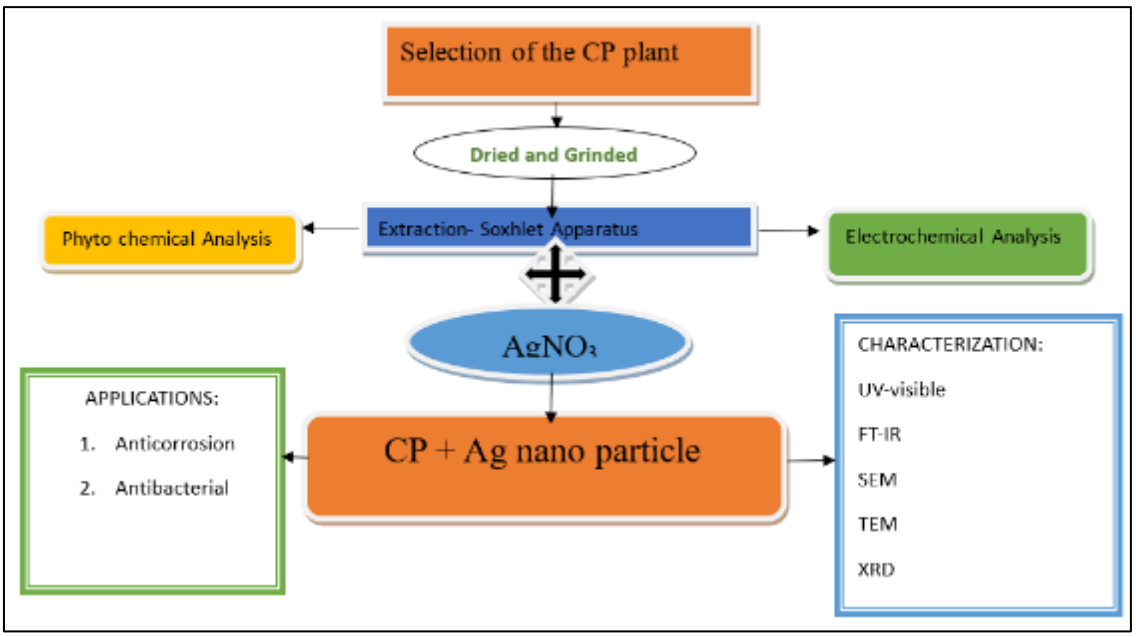

Figure 3 Schematic representation of the CP leaf extract silver nanoparticle process.

2.3. Characterization of Ag Nps

Chrozophora Plicata (CP) extract was characterized using the following primary techniques: Ag Nps were screened using UV-visible spectroscopy on a LABMAN LMSP-UV1200 with a wavelength precision of +0.5 nm. Using NICOLET 6700, USA instruments, a Fourier-transform infrared spectroscopy (FT-IR) investigation was conducted at Avinashilingam University Tamilnadu in India to verify the creation of green silver nanoparticles in the 450–400 cm-1 range.

To examine the structure of the recently produced Ag Nps, X-ray powder diffraction (X-RD) was performed using a model Xpert MPD. Cu target X-Ray tube, Cu Kα (λ ¼ 1.5406 A) radiation, and a tracking voltage of 40 KV were used to record the XRD patterns on an X-ray diffractometer in a range of 2θ from 30 to 1360. The exterior morphology of Ag Nps was investigated using Scanning Electron Microscopy (SEM-EDX). With an accelerating voltage of 0.2 to 30 kv and an emission current of 0–200 μA, a field emission scanning electron microscope was also utilized to examine the morphological characteristics of Ag Nps using a LaB6 filament 2 nm 30 KV and a W filament 3.5 nm at 30 kv. Using HR-TEM (model: Thermo-Scientific, Model: TALOS F200S G2, 200 KV, FEG) conducted in the TEM Lab, CNR Lab in Avinashilingam, Tamilnadu, the size, shape, and morphology of the produced Ag Nps were verified.

2.4. Theoretical studies

1-H-Pyrazol-3-amine and 2-(2-Diethylamino-ethoxy)-fluoren-9-one, two essential components of CB extract, were the subjects of quantum chemistry investigations. Essential details regarding the nature of the electron transfer property of 1-H-pyrazol-3-amine and 2-(2-Diethylamino-ethoxy)-fluoren-9-one can be found in various quantum chemical parameters derived from quantum chemical investigations. Thus, a theoretical analysis was conducted in the current investigation using the PM3 method and the Argus Lab (advanced version) software (Table 3).

Table 3 Quantum chemical results of higher amount of ingredients of the CP leaf extract which are acting as mild reducing agent Ag NPs synthesis.

Sno	compounds	ionization potential I	homo eV	lumo eV	energy gap eV	electn affinity (A = LUMO) eV	electronegativity χ = ((I+A)/2) eV	global hardness η= ((IA)/2) eV	softness (1/η)
1	1H-Pyrazol-3-amine	7.652489	-7.652	-0.056	7.596	0.056	3.8542445	3.7982445	0.2632795229
2	2-Diethylamino-ethoxy	7.369061	-7.369	-1.333	6.036	1.333	4.3510305	3.0180305	0.3313419132

HOMO, LUMO, electronegativity (χ), electrophilicity index (ω), chemical softness (σ), electron attraction (A), chemical potential (μ), ionization potential (I), and chemical hardness (η) are among the various quantum chemical characteristics that have been computed per the literature [46].

2.5. Antibacterial studies

According to past studies, plant-based silver nanoparticles shown strong antibacterial properties. At Avinashilingam University's Biogenics CN. Rao Centre for Research, gram-positive and gram-negative bacteria (E. coli and S. aureus) were found to be susceptible to the antibacterial activity of CP-synthesised Ag Nps. The zone of inhibition was evaluated during the analysis, which was carried out using the agar diffusion method. The antibiotic utilized is IC Ciprofloxacin, a common antibiotic and the solvent is DMSO. The stock cultures of bacteria were initially grown in broth media for eighteen hours at 37^0C before being transferred to the test tube. The previously mentioned media were used to create the agar plates and the wells inside the plate. During that time, each plate was shielded for 18 hours. Different amounts of nano-samples were arranged on plates, with a 20-minute gap between fills. Additional plates were incubated at 370C for 24 hours in order to determine the inhibitory zone's diameter, which was expressed in millimeters.

2.6. Corrosion test methods

In the present study, corrosion investigations were conducted using Fe metal of type Fe-410, which has chemical compositions of <0.15% C, 11.5-13.5% Cr, >0.75% Ni, <1.0% Mn, <1.0% Si, <0.04% P, and <0.03% S.

One centimeter of Fe metal pieces were exposed to the corrosive system, while the remaining portion was coated with epoxy resin for the Tafel plot and AC impedance spectroscopy techniques. The metal parts are cleaned with acetone and polished with sandpaper before testing. In the 1M HCl solution, the inhibitory effectiveness of Ag Nps against metal corrosion on the Fe surface was assessed using chemical (atomic absorption spectroscopy) and electrochemical (Tafel plot and AC impedance spectroscopy) methods. Using the SEM technique, surface analyses of Fe in a 1 molar HCl solution were conducted both with and without the ideal concentration of Ag Nps present. Atomic absorption spectroscopy (AAS) was used to measure the concentration of Fe (II) ions in the 1M HCl solution using the model GBC, 908, and Ag Nps at concentrations ranging from 1 mg/L to 4 mg/L. For this objective, one centimetre of polished iron metal was left exposed for ten hours in total. The amount of weight loss is then calculated by weighing Fe after it has been taken out of the corrosive solution and allowed to dry. The protection efficiency can be calculated as per the following expression.

$$\text{Protection efficiency (\%)} = \frac{B-A}{A} X100 \qquad (1)$$

Where, B-Amount of dissolved Fe (II) content without Ag Nps and A-Amount of dissolved Fe (II) content with Ag Nps

Utilizing a CHI 660C workstation, electrochemical calculations were performed utilizing three electrodes: platinum, calomel, and working cell (Fe). The AC impedance spectroscopy technique was used at frequencies between 105 and 102 Hz after a 30-minute stabilization period. At a scan rate of 1 mV/s, a potential between -0.20 and +0.20 V versus open circuit potential (OCP) is employed for the potentio-dynamic polarization (Tafel plots). The software that came with the CH instrument was used to obtain measurements of corrosion potential (Ecorr) and Tafel slopes. Based on the corrosion current density measurements, the polarization resistance (Rp) values were evaluated using the Stern-Geary equation [48].

Protection efficiency (%)= $1-R^0_{ct} / R_{ct} X100$ (2)

This expression can be used to determine protection efficiency based on the charge transfer resistance (from an AC impedance research) and the aluminum corrosion current density (from potentiodynamic polarization).
Where, R^0_{ct}= Charge transmission resistance value without Ag Nps and R_{ct} = Charge transfer resistance value with Ag Nps.

Inhibition Effiency (%)= $1-I_{corr} / I^0_{corr} X 100$ (3)

Where, I^0_{corr} -Fe corrosion current density (which was obtained from instrument) without Ag Nps and I_{corr} -Fe corrosion current density with Ag Nps. The morphology of Iron without and with 0.4 mg/L of Ag Nps was screened by scanning electron microscopy (SEM) technique at an immersion time of 5 h.

3. Results and discussion

The UV-visible spectroscopy method is typically used to analyze the optical and structural characteristics of nanoparticles. The color shift of the AgNO3 and plant extract mixture in the correct ratios allowed for control of the generated silver nanoparticles. After around 30 minutes, the two combinations' colors transitioned from green to yellow and finally to brown. The optical characteristics of the silver nanoparticles caused these color changes. SPR peaks, a feature of noble metals that arise when the free-moving electrons in Ag Nps come into contact with visible or ultraviolet light, were the cause of this.

Different absorption bands cause Ag Nps to vary in size and form, in accordance with Mie's hypothesis of colloidal particles. Two or three absorption bands at 742 nm offer a perfect triangle, as reported by Chen and Carroll, whereas at 465 nm, triangular forms are indicated, as reported by Chalmers, Griffiths, Farooq et al. The UV-visible spectrum also exhibits anisotropic character. Quadrupole resonance outside the plane is linked to the same time at 333 nm. Two significant bands, one at 280 nm and the other at 450 nm, were discovered in the current investigation. After adding the extract, we also experimented with the time gap of AgNP production, recording UV visible spectra every five minutes. It's interesting to note that neither peak's wavelengths shift considerably. Figure 5a shows the produced silver nanoparticles' well-defined SPR band at 450 nm. About 450 nm of absorbance verifies that Ag Nps have formed. Time-dependent increases in the SPR band also show that additional Ag Nps are forming in the solution.

Individual metal particle size and shape are also represented by this band. A leaf extract used to decrease and cap the Ag Nps was used to identify secondary phyto-medicines using Fourier transform infrared (FT-IR) spectroscopy. Fig. 5b displays the FT-IR spectra of Ag Nps. The Ag Nps' primary absorption bands were 3927.07 cm^{-1},3749.62cm^{-1},3348.42cm^{-1},1635.64 cm^{-1}. It is recommended that certain polyphenolic compounds be connected to the silver nanoparticles because the band at 3348.12 cm^{-1} can be allocated for –NH/-OH vibration stretching and the band around 1635.64 cm^{-1} is assigned for stretching vibration of carbon-carbon. These FT-IR bands of amine, alcoholic and carbonyl groups, which are necessary for the capping of produced silver nanoparticles, may be the cause of the synthesis of hybrid Ag Nps [10–12].

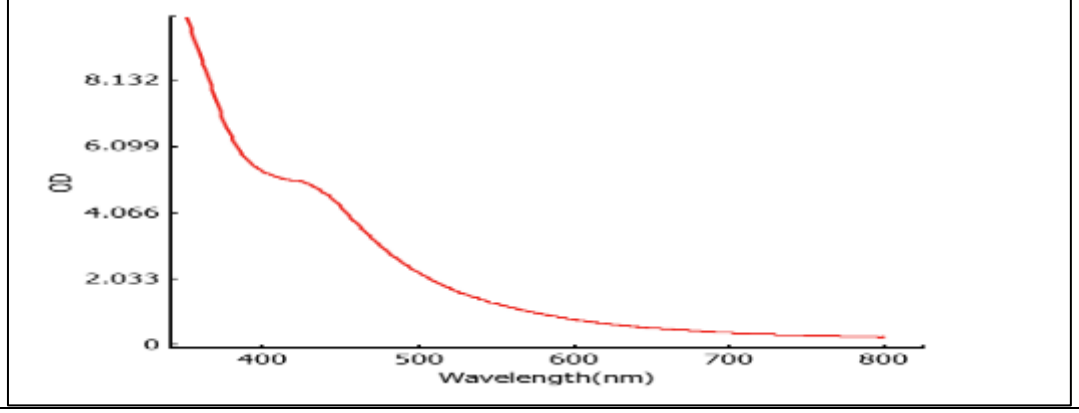

(a)

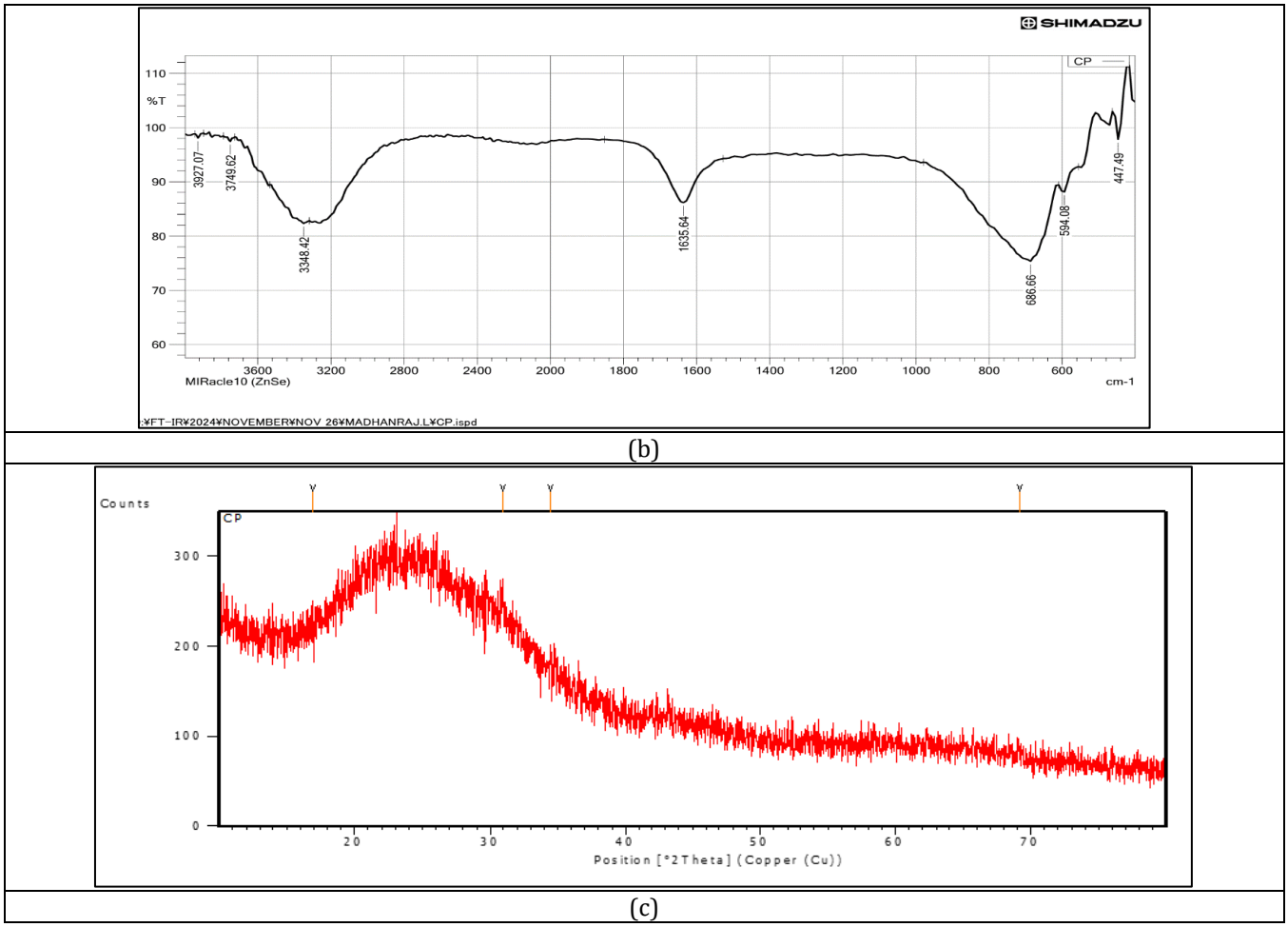

Figure 4 (a–c): (a) UV–Visible spectrum, (b) FT-IR spectrum and (c) XRD results of Ag Nps.

The XRD technique is used to confirm the crystalline/amorphous nature of newly synthesized Ag Nps. The crystallite size (L) of green Ag Nps was evaluated with the help of the Scherrer equation, as shown below:

$$L = B\lambda/\beta cos\ \theta \qquad (4)$$

where, β - full-width half maximum of diffraction, B - Scherer constant, θ - Bragg's angle, and λ – wavelength.

Fig. 4.c shows the XRD pattern of Ag Nps. The well-resolved, high-intensity peaks at 2θ = 38.270, 44, 63.360, and 76.120 in their X-ray diffraction (XRD) pattern demonstrate the crystal lattice structure of Ag Nps. The literature analysis indicates that the typical peaks for Ag Nps are 2θ = 38.1630, 43.5970, and 76.5440 [13–15]. This illustrates how Ag+ ions can create new silver nanoparticles with the help of AS extract. The spectra at the (111), (200), and (311) planes, respectively, show the silver nanoparticles' Face Cantered Cubic (FCC) and crystalline structure. The preferred orientation of Ag Nps is the (111) plane, as indicated by a high-intensity peak at 2ɬ = 38.270 [12, 15–17]. The Scherer equation showed that Ag Nps' average diameter ranged from 16 to 65 nm.

Energy Dispersive X-ray (EDX) constituent elemental analysis revealed a significant concentration of physiologically generated Ag Nps, as shown in Fig. 6. The purity and chemical makeup of Ag NPs show that a sizable amount of silver metal was first produced with other elements. When paired with relative oxygen, silicon, and potassium compositions, silver forms an organic capping agent that binds to the surface of Ag NPs. To examine the distribution of Ag NPs' particle size pattern, the diameters of a minimum of 100 particles were determined using HRTEM pictures. The HRTEM results are shown in Fig. 5. The spherical Ag particle structures are confirmed by HRTEM pictures. The typical size range of Ag NPs nanoparticles is 15–25 nm. The greatest particle size distributions range in diameter from 35 to 60 nm.

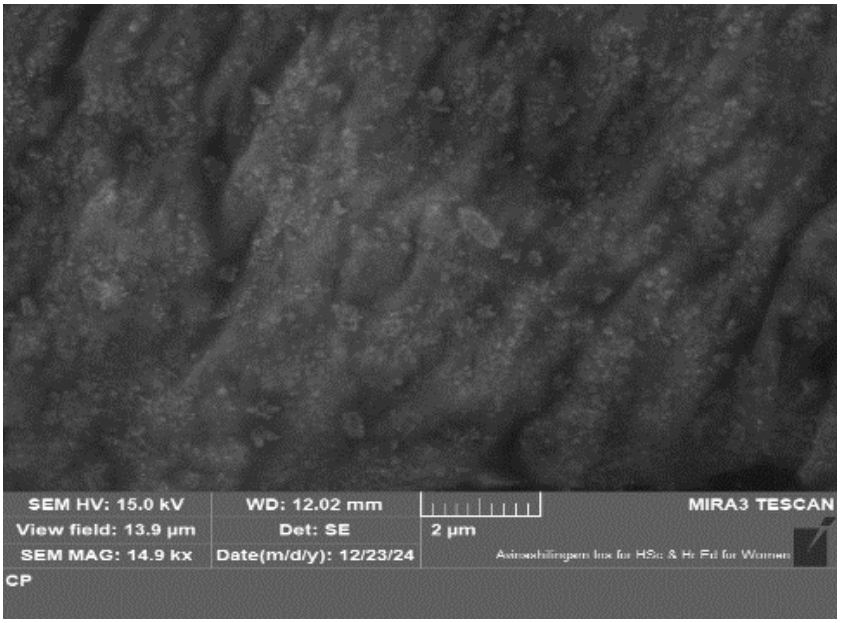

Figure 5 HRTEM images of Ag NPs

For a range of packaging and pharmaceutical applications, research on Ag NPs' antibacterial qualities is essential. The data on antibacterial activity are shown in Fig. 7. It has antibacterial qualities against Staphylococcus aureus and Escherichia coli, two round, Gram-positive bacteria. In this study, gram-negative bacteria, including E. coli, are displayed. As the surface area of silver nanoparticles increases, so does the number of atoms at the surface. The high stability of the nanoparticles indicates that higher concentrations of phytochemicals act as more potent reducing agents. The pictures in Figure 6 demonstrate the highest level of antibacterial activity. The optimal zone of inhibition occurs between 500 and 1000 µg of clear zone. Small microorganisms interacted with silver nanoparticles and were readily captured on this huge surface area [49]. Silver nanoparticles' ultra-small size—roughly 200 times smaller than that of bacteria—creates an electrostatic attraction between the microbial surface and the nanoparticles, rendering the bacteria inactive by trapping them with essential enzymes that contain thiol groups.

This raises the particles' antibacterial efficacy [48–52] and interferes with the bacterial cells' regular activity, which eventually leads to cell death [50]. All of these elements help to explain the antibacterial activity [17–20], and the shape of the generated silver nanoparticles also matters [53]. The activity is more noticeable for gram-negative bacteria, with a zone of inhibition measured shown to be good with bacteria Escherichia. Coli at 1000 µg/ml [54–57]. Same time results also shown that Ag Nps have no vital antibacterial effect on Staphylococcus aureus strain [16, 18, 19].

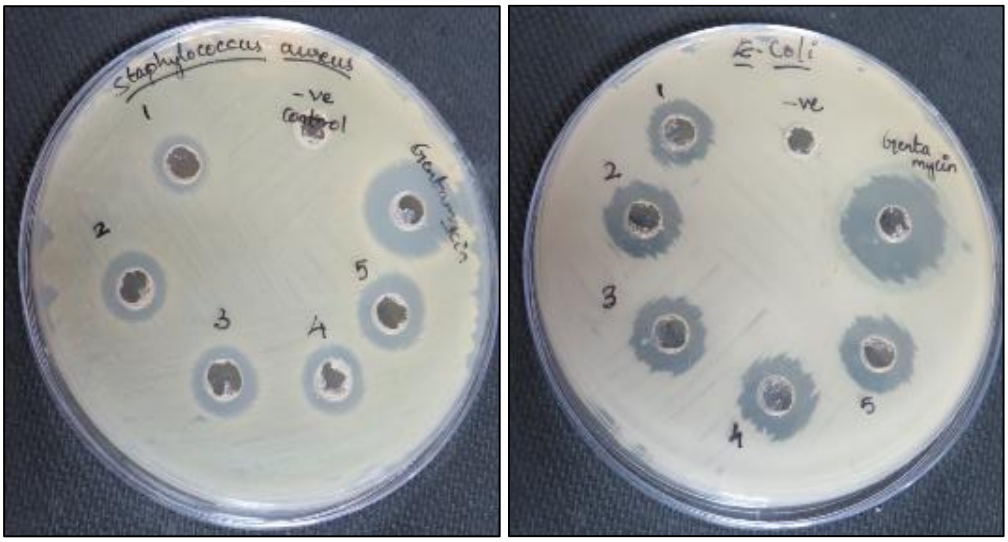

Figure 6 Plates showing Antibacterial activity of AS extract and Ag NPs

There is ongoing discussion over the exact mechanism by which silver nanoparticles work to inhibit microorganisms. The electrostatic interaction may possibly account for this. The medium, area, and shape are crucial factors to take into account when forecasting the antibacterial efficacy of silver nanoparticles. Furthermore, the permeable cell membrane kills the bacteria when they come into touch with the free radicals produced by the silver nanoparticles.

The atomic absorption spectroscopy (AAS) method was used to investigate the beneficial impact of Ag NPs on the anti-corrosion of iron in the experimental solution. The pre-weighed Fe coupon was submerged in a 1M HCl solution with and without Ag NPs for 10 hours at 3030 C during the experiment. When the Fe electrode is removed from the 1M HCl solution, the weight loss is then recorded using a digital analytical balance that is connected to the computer. The results of the AAS are shown in Table 4. The table showed how strongly the Ag NPs adhered to the Fe surface in the experimental solution. Ag Nps at concentrations of 1 mg/L, 2 mg/L, 3 mg/L, and 4 mg/L in 1 M HCl solution decreased the Fe weight loss, as shown in Table 4. A higher protection rate is the consequence of the increased surface coverage of green nanoparticles over the Fe surface in the experimental solution caused by the increased absorption of Ag Nps. Ag Nps' adsorption across the Fe surface creates a hedge for the transfer of mass and charge, which lessens the interaction between the Fe surface and the 1M HCl solution.

The Ag Nps' strong adhesion to the Fe surface in the experimental solution was displayed in the table. Ag Nps at concentrations of 1 mg/L, 2 mg/L, 3 mg/L, and 4 mg/L in 1 M HCl solution decreased the Fe weight loss, as shown in Table 4. A higher protection rate is the consequence of the increased surface coverage of green nanoparticles over the Fe surface in the experimental solution caused by the increased absorption of Ag Nps. Ag Nps' adsorption across the Fe surface creates a hedge for the transfer of mass and charge, which lessens the interaction between the Fe surface and the 1 M HCl solution. The breakdown of the Fe surface is prevented by the presence of an Ag Nps coating on it. The adsorption of electron-rich elements on the empty or partially filled orbits of Fe in the 1 M HCl solution may be linked to the protective effectiveness of Ag Nps on the Fe surface. Consequently, the newly formed bonds with the green nanoparticles are more stable.

Table 4 Atomic Absorption Spectroscopic results

Concentration (mg/L)	**Weight loss of Iron in grams after 10 h immersion period**	**Protection efficiency (%)**
Bare	28×10^{-3}	-
0.1	1.6×10^{-3}	92
0.2	1.4×10^{-3}	94
0.3	6.9×10^{-4}	95
0.4	0.8×10^{-4}	97

AC impedance spectroscopy can be used to determine the reaction kinetics at the Ferrous/1 M HCl solution interface. Fig. 6(a) displays the Nyquist curves that were obtained from the inhibition of Fe corrosion with CP-Ag NP concentrations ranging from 1 mg/L to 4 mg/L. The Nyquist readings for the different readings are shown in Table 5. Except for the diameter of the depressed semi-circle, the protected system's Nyquist plots (impedance curves) are identical to those of the unprotected system.

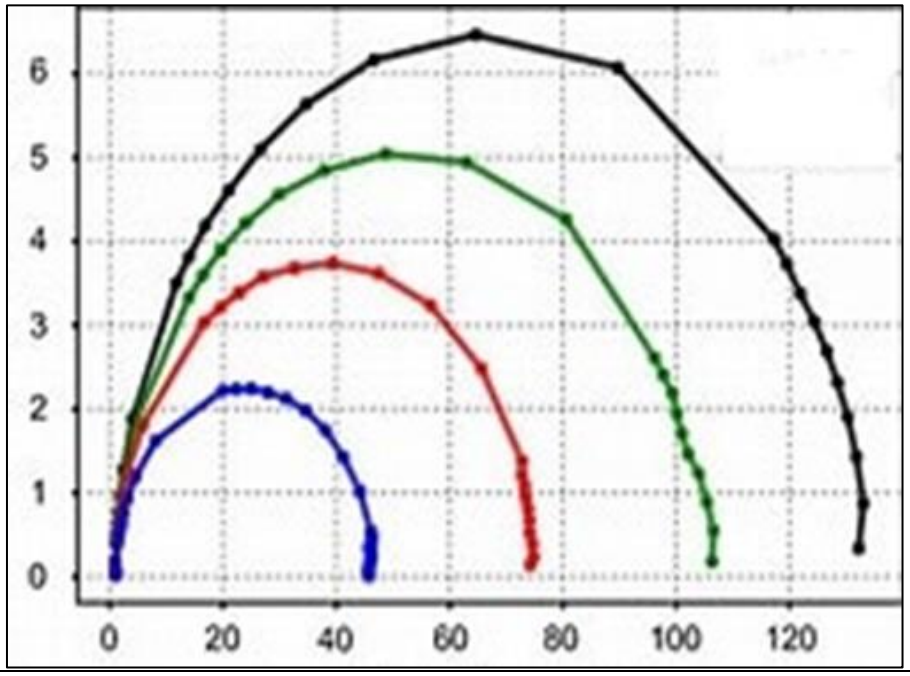

(a)

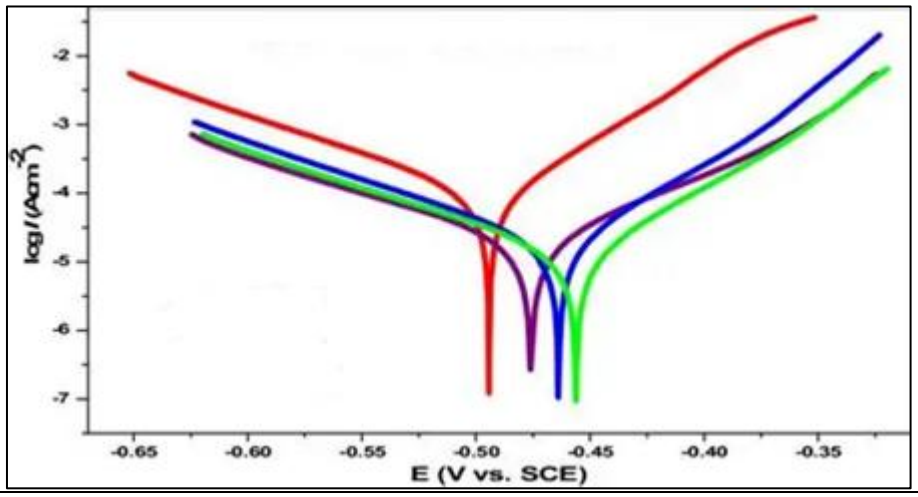

(b)

Figure 7 (a - b) (a) Nyquist plots in the absence and presence of corrosion inhibitor, (b) Tafel plots without and with corrosion inhibitor

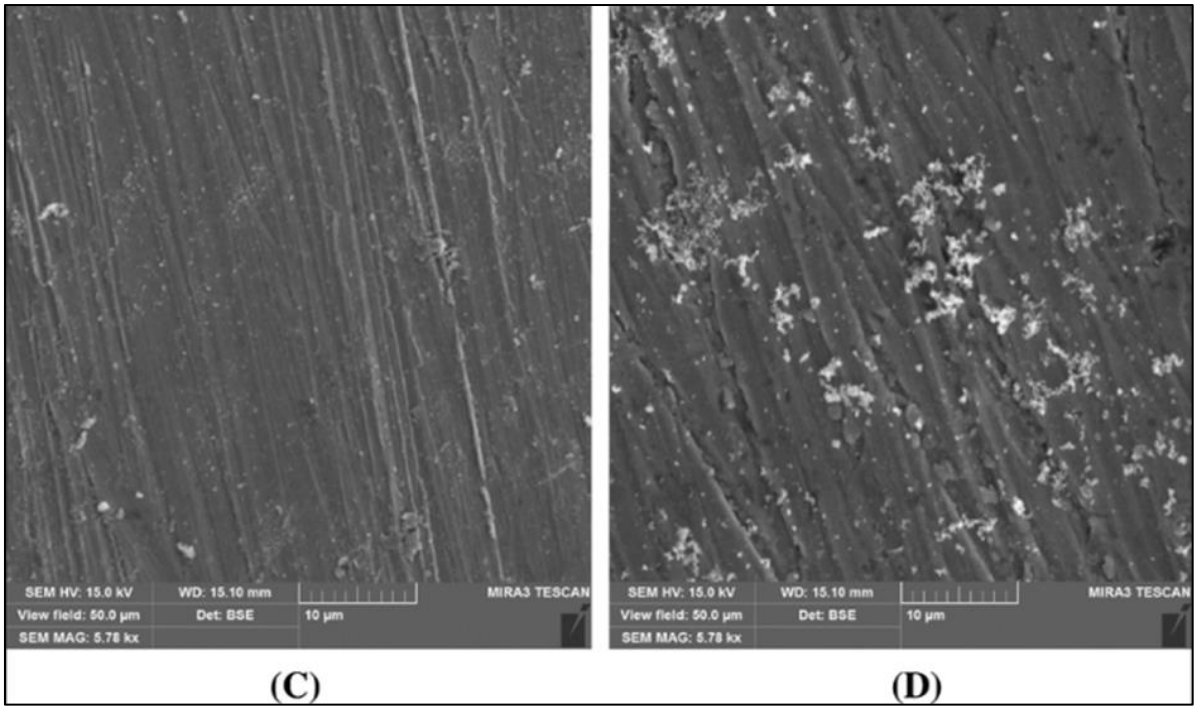

Figure 7 (c - d) SEM images without and with silver nanoparticles

Table 5 Impedance spectroscopy results

Concentration Mg/L	N	R_{ct} (ohm)	X^2	Inhibition efficiency
Bare	0.9156	13.32	0.0000183	-
0.1	0.8675	168.1	0.0000681	92.1
0.2	0.8787	172.5	0.000043	91.1
0.3	0.8961	179.3	0.0000941	92.3
0.4	0.6896	228.7	0.0000456	93.6

The Nyquist plots in Fig. 7(a) show that the presence and absence of CP Ag NPs (Only extract) are not a perfect semicircle because of frequency dispersion. There is a substantial correlation between the charge transfer capability values and the concentration of Ag NPs in the sample solution. As the concentration of the compound rises from 1 mg/L to 4 mg/L, the rate of ferrous corrosion decreases and the charge transfer resistance values improve. As the dosage of Ag NPs increases, the radius of the depressed semicircle grows as well, providing strong evidence that the compound inhibits the dissolution of Fe in the 1M HCl solution. The formation of a barrier protective layer on the Fe surface significantly slows down the rate of disintegration. This table makes it evident that the charge transfer resistance values and the concentration of Ag Nps in solution are negatively correlated. Charge transfer resistance values rise with increasing Ag NP content, indicating Ag NPs' anticorrosive action over the electrode surface in the 1M HCl solution.

Figure 7 (b) displays the ferrous polarization graphs in a 1 M HCl solution with four distinct Ag NP dosages. Table 6 tabulates the results. Ferrous corrosion current density values were shown to be significantly impacted by the addition of green nanoparticles, with a lower ferrous corrosion current density value occurring at greater Ag NP concentrations. The surface area of Fe covered by Ag NPs species rises as Ag NPs levels rise, suggesting that the main mechanism of ferrous protection is the adsorption of green nanoparticles over the Fe surface. The interaction between the Fe and the solution media is restricted by the layer of Ag NPs that develops on top of the Fe surface. wherein silver nanoparticles serve as the anticorrosion agent. Additionally, the absence of a discernible change in the Ecorr, anodic, or cathodic Tafel slope values [9, 23] indicates the mixed corrosion prevention property of the Ag NPs over the iron surface in the 1M HCl solution.

Table 6 Results obtained from Tafel plot

Concentration (mg/ L)	Corrosion potential (E corr) (mV)	Anodic Tafel slope (V/ dec)	Cathodic Tafel slope (V/ dec)	Corrosion current (µA/ cm^2)	Protection efficiency (%)
Bare	-761	0.03	6.36	551	-
0.1	-718	5.22	4.73	117	88.2%
0.2	-712	5.46	4.71	109	90.4%
0.3	-724	5.58	4.76	106	90.6%
0.4	-711	5.41	4.70	101	90.9%

4. Conclusions

Stable Ag NPs were successfully created in the present study using a green technique using c leaf extract, producing sphere-shaped particles with sizes ranging from 16 to 65 nm. CP extract was used to create silver nanoparticles for the first time. They exhibit exceptionally potent antibacterial action against E. coli. Tests were also conducted on the anti-corrosion capabilities of CP extract. The protection efficiency values obtained from the three techniques (AAS, Tafel plot, and impedance spectroscopy) increased in tandem with the dosage of nanoparticle concentration. The highest protection efficiency value (97%) was attained by employing the AAS technique. Following the use of Ag NPs, surface morphological changes were noticed by SEM, and these changes are associated with the AAS, Tafel plot, and impedance data. These new characteristics of Ag NPs demonstrate that the bio-waste *Chrozophora Plicata* plant can be used as a potential source for large scale synthesis of Ag Nps with biological applications in the future.

Abbrevations

- CP- Chrozophora Plicata
- CP-Ag Nps Chrozophora Plicata extract silver nanoparticles
- Ag Nps- silver nanoparticles
- NP's -Nanoparticles
- UV/Vis Ultraviolet–Visible spectroscopy
- FTIR -Fourier-Transform Infrared Spectroscopy
- XRD -X-ray Diffraction
- SEM- Scanning electron microscopy
- SEM-EDX Scanning Electron Microscopy- Energy-dispersive X-ray spectroscopy
- HRTEM -High-Resolution Transmission Electron Microscopy
- E. coli -Escherichia. Coli S. aureus Staphylococcus aureus
- $AgNO_3$ -Silver nitrate
- 1M HCl -One molar hydrochloric acid
- AAS- Atomic Absorption Spectroscopy - 0.01 N: 0.01 Normal
- Fe- Metal Ferrous metal
- OCP- Open circuit potential
- FCC -Face Centred Cubic
- Ecorr-Corrosion mg/L: milligram per litre

Compliance with ethical standards

Acknowledgments

The authors thank the principal and Head of the institutions for their moral support.

Disclosure of conflict of interest

The authors declare that there is no conflicts of interest

Authors declaration

I confirm that I have read, understand, and agreed to the submission guidelines, policies, and submission declaration of the journal. I confirm that all authors of the manuscript have no conflict of interest to declare. I confirm that the manuscript is the author's original work and the manuscript has not received prior publication and is not under consideration for publication elsewhere. On behalf of all Co-Authors, I shall bear full responsibility for the submission. I confirm that all authors listed on the title page have contributed significantly to the work, have read the manuscript, attest to the validity and legitimacy of the data and its interpretation, and agree to its submission. I confirm that the paper now submitted is not a copied or plagiarized version of some other published work. I declare that I shall not submit the paper for publication in any other Journal or Magazine till the decision is made by journal editors. If the paper is finally accepted by the journal for publication, I confirm that I will either publish the paper immediately or withdraw it according to withdrawal policies. I understand that submission of false or incorrect information would invite appropriate penal actions as per rules of the journal and UGC guidelines. I confirm that **no funding** is provided.

Data Availability Statement

The data that support the findings of this study are available from the corresponding author upon reasonable request.

References

[1] Nayak D, Ashe S, Rauta PR, et al. Bark extract mediated green synthesis of silver nanoparticles: Evaluation of antimicrobial activity and antiproliferative response against osteosarcoma. Mater Sci Eng C. 2016; 58:44–52.

[2] Nalwa HS. Handbook of nanostructured materials and nanotechnology. New York (NY): Academic Press; 1999.

[3] Nasrollahzadeh M, Sajadi SM. Synthesis and characterization of titanium dioxide nanoparticles using Euphorbia heteradenaJaub root extract and evaluation of their stability. Ceramics Int. 2015; 41:14435–14439.

[4] Zulfiqar U, Subhani T, Husain SW. Synthesis and characterization of silica nanoparticles from clay. J Asian Ceramic Soc. 2016; 4:91–96.

[5] Fazlzadeh M, Rahmani K, Zarei A, et al. A novel green synthesis of zero valent iron nanoparticles (NZVI) using three plant extracts and their efficient application for removal of Cr(VI) from aqueous solutions. Adv Powder Technol. 2017; 28:122–130.

[6] Mittal AK, Chisti Y, Banerjee UC. Synthesis of metallic nanoparticles using plant extracts. Biotechnol Adv. 2013; 31:346–356.

[7] Santhoshkumar J, Kumar SV, Rajeshkumar S. Synthesis of zinc oxide nanoparticles using plant leaf extract against urinary tract infection pathogen. Resource-Efficient Technol. 2017; 05:001.

[8] Logeswari P, Silambarasan S, Abraham J. Synthesis of silver nanoparticles using plants extract and analysis of their antimicrobial property. J Saudi Chem Soc. 2015; 19:311–317.

[9] Rasheed T, Bilal M, Iqbal HM, et al. Green biosynthesis of silver nanoparticles using leaves extract of Artemisia vulgaris and their potential biomedical applications. Coll Surf B Biointerf. 2017; 158:408–415.

[10] Bell MR. A case for nanomaterials in the oil and gas exploration and production business.In: International Congress of Nanotechnology (ICNT). 2004 Nov; 7–10.

[11] Lau HC, Yu M, Nguyen QP. Nanotechnology for oilfield applications: challenges and impact. J Petroleum Sci Eng. 2017; 157:1160–1169.

[12] Paydar P, Ahmadi M. Characteristics of water-based drilling mud containing Gilsonite with Boehmite nanoparticles. Bulletin de laSociété Royale des Sciences de Liège. 2017; 86:248–258.

[13] Abdo J, Haneef MD. Clay nanoparticles modified drilling fluids for drilling of deep hydrocarbon wells. Appl Clay Sci. 2013; 86:76–82.

[14] Fakoya MF, Shah SN. Emergence of nanotechnology in the oil and gas industry: Emphasis on the application of silica nanoparticles. Petroleum. 2017; 03:001.

[15] Ponmani S, Nagarajan R, Sangwai J. Applications of nanotechnology for upstream oil and gas industry. J Nano Res. 2013; 24:7–15.

[16] Bera A, Belhaj H. Application of nanotechnology by means of nanoparticles and nanodispersions in oil recovery – a comprehensive review. J Nat Gas Sci Eng. 2016; 34:1284–1309.

[17] Ganachari S.V, Deshpande R, Bhat R, Rao N.V.S, Huh D.S, Venkataraman A. Green synthesis silver nanoparticles via Eichhornia Crassipes leaves extract and their applications, J. Bionanoscience. 2011; 5:107.

[18] Mokashi A.U, Ganachari S.V, Yaradoddi J.S, Tapaskar R.P, Banapurmath N.R, Shettar A.S. Synthesis and Characterization of Nano Strontium Ferrite and its gas sensing studies, IOP Conf. Ser. Mater. Sci. Eng, 2018; 376:012055.

[19] Mulvihill M.J, Beach E.S, Zimmerman J.B, Anastas P.T. Green Chemistry and Green Engineering: A Framework for Sustainable Technology Development. Annu. Rev. Environ. Resour. 2011; 36:271.

[20] Gour A, Jain N.K. Advances in green synthesis of nanoparticles. Artificial Cells, Nanomedicine, and Biotechnology. 2019; 47:844.

[21] Akter M, Md Rahman M, Ullah A.K.M.A, Md Sikder T, Hosokawa T, Saito T, Kurasaki M. Brassica rapa var. japonica Leaf Extract Mediated Green Synthesis of Crystalline Silver Nanoparticles and Evaluation of Their Stability, Cytotoxicity and Antibacterial Activity.. Inorg. Organomet. Polym. 2018; 28:1483.

[22] Mohammed A.E, Al-Qahtani A, Al-Mutairi A, Al-Shamri B, Aabed K. Antibacterial and Cytotoxic Potential of Biosynthesized Silver Nanoparticles by Some Plant Extracts. Nanomaterials. 2018; 8:382. Antibacterial and Cytotoxic Potential of Biosynthesized Silver Nanoparticles by Some Plant Extracts. 7 May 2018 / Revised: 19 May 2018 / Accepted: 26 May 2018 / Published: 30 May 2018.

[23] Raghavendra N, Bhat J.I. Red Arecanut Seed Extract as a Sustainable Corrosion Inhibitor for Aluminum Submerged in Acidic Corrodent: An Experimental Approach Towards Zero Environmental Impact, Period. Polytech. - Chem. Eng. 2018; 62:351.

[24] Lakshmanan G, Sathiyaseelan A, Kalaichelvan P.T, Murugesan K, Karbala, Plant-mediated synthesis of silver nanoparticles using fruit extract of Cleome viscosa L.: Assessment of their antibacterial and anticancer activity. International Journal of Modern Science. 2018; 4:61.

[25] Gunnarsson C.C, Petersen C.M. Water hyacinths as a resource in agriculture and energy production: A literature review. Waste Manag. 2007; 27:117.

[26] Buanafina M.M de O, Buanafina M.F, Dalton S, Morris P, Kowalski M, Yadav M.K, Capper L. Probing the role of cell wall feruloylation during maize development by differential expression of an apoplast targeted fungal ferulic acid esterase. PLoS One. 2020; 15:0240369.

[27] Kumar N, Pruthi V. Potential applications of ferulic acid from natural sources. Biotechnology Reports. 2014; 4:86.

[28] Khan M.J, Shameli K, Sazili A.Q, Selamat J, Kumari S. Rapid Green Synthesis and Characterization of Silver Nanoparticles Arbitrated by Curcumin in an Alkaline Medium. Molecules. 2019; 24(4):719.

[29] Khatami M, Sharifi I, Nobre M.A.L, Zafarnia N, Aflatoonian M.R. Waste-grass-mediated green synthesis of silver nanoparticles and evaluation of their anticancer, antifungal and antibacterial activity Green Chem. Lett. Rev. 2018; 11:125.

[30] Hembram K.C, Kumar R, Kandha L, Parhi P.K, Kundu C.N, Bindhani B.K. Therapeutic prospective of plant-induced silver nanoparticles: application as antimicrobial and anticancer agent. Artif Cells Nanomed Biotechnol. 2018; 46:S38.

[31] Nasar M.Q, Khalil A.T, Ali M, Shah M, Ayaz M, Shinwari Z.K. Phytochemical Analysis, Ephedra Procera C. A. Mey. Mediated Green Synthesis of Silver Nanoparticles, Their Cytotoxic and Antimicrobial Potentials. Medicina. 2019; 55:369.

[32] Raghavendra N, Ishwara Bhat J. An Environmentally Friendly Approach Towards Mitigation of Al Corrosion in Hydrochloric Acid by Yellow Colour Ripe Arecanut Husk Extract: Introducing Potential and Sustainable Inhibitor for Material Protection. J Bio Tribo Corros. 2017; 4:2.

[33] Fatimah I, Aftrid Z.H.V.I. Characteristics and antibacterial activity of green synthesized silver nanoparticles using red spinach (Amaranthus Tricolor L.) leaf extract. Green Chem. Lett. Rev. 2019; 12:25.

[34] Alfuraydi A.A, Devanesan S, Al-Ansari M, AlSalhi M.S, Ranjitsingh A.J Eco-friendly green synthesis of silver nanoparticles from the sesame oil cake and its potential anticancer and antimicrobial activities. Photochem. Photobiol. B Biol. 2019; 192:83.

[35] Behravan M, Hossein Panahi A, Naghizadeh A, Ziaee M, Mahdavi R, Mirzapour A. Facile green synthesis of silver nanoparticles using Berberis vulgaris leaf and root aqueous extract and its antibacterial activity. Int. J. Biol. Macromol. 2019; 124:148.

[36] Jogaiah S, Kurjogi M, Abdelrahman M, Hanumanthappa N, Tran L.S.P. Ganoderma applanatum-mediated green synthesis of silver nanoparticles: Structural characterization, and in vitro and in vivo biomedical and agrochemical properties. Arabian Journal of Chemistry. 2019; 12:1108.

[37] Arya G, Kumari R.M, Gupta N, Kumar A, Chandra R, Nimesh S. Green synthesis of silver nanoparticles using Prosopis juliflora bark extract: reaction optimization, antimicrobial and catalytic activities, Artificial Cells. Nanomedicine, and Biotechnology. 2018; 46:985.

[38] Kumar V, Singh S, Srivastava B, Bhadouria R, Singh R. Green synthesis of silver nanoparticles using leaf extract of Holoptelea integrifolia and preliminary investigation of its antioxidant, anti-inflammatory, antidiabetic and antibacterial activities. Journal of Environmental Chemical Engineering. 2019; 7:103094.

[39] Mousavi B, Tafvizi F, Zaker S. Bostanabad, Green synthesis of silver nanoparticles using Artemisia turcomanica leaf extract and the study of anti-cancer effect and apoptosis induction on gastric cancer cell line (AGS), Artificial Cells. Nanomedicine and Biotechnology. 2018; 46:499.

[40] Singh C, Kumar J, Kumar P, Chauhan B.S, Tiwari K.N, Mishra S.K, Srikrishna S, Saini R, Nath G, Singh J. Green synthesis of silver nanoparticles using aqueous leaf extract of Premna integrifolia (L.) rich in polyphenols and evaluation of their antioxidant, antibacterial and cytotoxic activity. Biotechnol. Biotechnol. Equip. 2019; 33:359.

[41] Erci F, Cakir-Koc R, Isildak I. Green synthesis of silver nanoparticles using Thymbra spicata L. var. spicata (zahter) aqueous leaf extract and evaluation of their morphology-dependent antibacterial and cytotoxic activity, Artificial Cells. Nanomedicine, and Biotechnology. 2018; 46:150.

[42] Hamelian M, Zangeneh M.M, Amisama A, Varmira K, Veisi H. Green synthesis of silver nanoparticles using Thymus kotschyanus extract and evaluation of their antioxidant, antibacterial and cytotoxic effects. Appl. Organomet. Chem. 2018; 32:4458.

[43] Rorong J.A, Sudiarso S, Prasetya B, Polii-Mandang J, Suryanto E. Phytochemical Analysis of Eceng Gondok (Eichhornia Crassipessolms) Of Agricultural Waste as Biosensitizer for Ferri Photoreduction, AGRIVITA. Journal of Agricultural Science. 2012; 34:152.

[44] David A.V.A, Arulmoli R, Parasuraman S. Rapid analysis of flavonoids based on spectral library development in positive ionization mode using LC-HR-ESI-MS/MS. Phcog. Rev. 2016; 10.

[45] Lalitha P, Sripathi S.K, Jayanthi P. Secondary Metabolites of Eichhornia crassipes (Waterhyacinth). Natural Product Communications. 2012; 7.

[46] Kavitha V, GunavathyComputational N. Investigations on Curcumin and Demethoxycurcumin as Corrosion Inhibitors: A Comparative Analysis. International Journal of Science & Engineering. 2017; 2(3):2456-3315.

[47] Stern M, Geary A.L. Electrochemical Polarization: I. A Theoretical Analysis of the Shape of Polarization Curves. J. Electrochem. Soc. 1957; 104:56.

[48] Yugay Y.A, Usoltseva R.V, Silant'ev V.E, Egorova A.E, Karabtsov A.A, Kumeiko V.V, Ermakova S.P, Bulgakov V.P, Shkryl Y.N. Synthesis of bioactive silver nanoparticles using alginate, fucoidan and laminaran from brown algae as a reducing and stabilizing agent. Carbohydr. Polym. 2020; 245:116547.

[49] Islam N.U, Jalil K, Shahid M, Rauf A, Muhammad N, Khan A, Shah M.R, Khan M.A. Green synthesis and biological activities of gold nanoparticles functionalized with Salix alba. Arabian Journal of Chemistry. 2019; 12:2914.

[50] Raghavendra N, Ishwara Bhat J. Inhibition of Al corrosion in 0.5 M HCl solution by Areca flower extract. Journal of King Saud Universit, - Engineering Sciences. 2019; 31:202.

[51] Singh J, Dhaliwal A.S. Novel Green Synthesis and Characterization of the Antioxidant Activity of Silver Nanoparticles Prepared from Nepeta leucophylla Root Extract. Anal. Lett. 2019; 52:213.

[52] Mathew S, Prakash A, Radhakrishnan E.K. Sunlight mediated rapid synthesis of small size range silver nanoparticles using Zingiber officinale rhizome extract and its antibacterial activity analysis. Inorganic and Nano-Metal Chemistry. 2018; 48:139.

[53] Guimar~aes M.L, da Silva F.A.G, da Costa M.M, de Oliveira H.P. Green synthesis of silver nanoparticles using Ziziphus joazeiro leaf extract for production of antibacterial agents. Appl. Nanosci. 2020; 10:1073.

[54] Jones R.S, Draheim R.R, Roldo M. Silver Nanowires: Synthesis, Antibacterial Activity and Biomedical Applications. Appl. Sci. 2018; 8:673.

[55] Sumitha S, Vasanthi S, Shalini S, Chinni S.V, Gopinath S.C.B, Anbu P, Bahari M.B, Harish R, Kathiresan S. V. Ravichandran, Phyto-Mediated Photo Catalysed Green Synthesis of Silver Nanoparticles Using Durio Zibethinus Seed Extract: Antimicrobial and Cytotoxic Activity and Photocatalytic, Applications. Molecules 2018; 23:3311.

[56] Roy A, Bulut O, Some S, Mandal A.K, Yilmaz M.D. Green synthesis of silver nanoparticles: biomolecule-nanoparticle organizations targeting antimicrobial activity. RSC Adv. 2019; 9:2673.

[57] Chand K, Abro M.I, Aftab U, Shah A.H, Lakhan M.N, Cao D, Mehdi G, Mohamed A.M.A. Green synthesis characterization and antimicrobial activity against Staphylococcus aureus of silver nanoparticles using extracts of neem, onion and tomato. RSC Adv. 2019; 9:17002.

[58] Femi-Adepoju A.G, Dada A.O, Otun K.O, Adepoju A.O, Fatoba O.P. Green synthesis of silver nanoparticles using terrestrial fern (Gleichenia Pectinata (Willd.) C. Presl.): characterization and antimicrobial studies. Heliyon. 2019; 5:01543.

[59] Otunola G.A, Afolayan A.J. In vitro antibacterial, antioxidant and toxicity profile of silver nanoparticles green-synthesized and characterized from aqueous extract of a spice blend formulation, Biotechnol. Biotechnol. Equip. 2018; 32:724.